

## SHORT COMMUNICATION

# Maximization of conversion efficiency based on global normal irradiance using hybrid concentrator photovoltaic architecture

Noboru Yamada\* and Daiki Hirai

Department of Mechanical Engineering, Nagaoka University of Technology, Nagaoka, Japan

## ABSTRACT

Maximization of module conversion efficiency based on global normal irradiance (GNI) rather than direct normal irradiance (DNI) was experimentally demonstrated using a hybrid concentrator photovoltaic (CPV) architecture in which a low-cost solar cell (a bifacial crystalline silicon cell) was integrated with a high-efficiency concentrator solar cell (III–V triple-junction cell) to harvest diffuse sunlight. The results of outdoor experiments showed that the low-cost cell enhanced the generated power by factors of 1.39 and 1.63 for high-DNI and midrange-DNI conditions, respectively, and that the resultant GNI-based module efficiencies were 32.7% and 25.6%, respectively. © 2016 The Authors. *Progress in Photovoltaics: Research and Applications* published by John Wiley & Sons Ltd.

## KEYWORDS

concentrator photovoltaic; module design; multi-junction solar cells; crystalline silicon solar cells; bifacial solar cells

### \*Correspondence

Noboru Yamada, Department of Mechanical Engineering, Nagaoka University of Technology, Nagaoka, Japan.

E-mail: noboru@nagaokaut.ac.jp

This is an open access article under the terms of the Creative Commons Attribution-NonCommercial License, which permits use, distribution and reproduction in any medium, provided the original work is properly cited and is not used for commercial purposes.

Received 23 July 2015; Revised 27 January 2016; Accepted 1 February 2016

## 1. INTRODUCTION

Improving terrestrial photovoltaic conversion efficiency is an essential and urgent issue in mitigating climate and energy crises in the coming decades. Multi-junction (MJ) concentrator solar cells have the highest theoretical limit among the available solar cells [1] and produce the highest cell conversion efficiencies—currently in excess of 40% and eventually expected to reach 50% [2–5]. Field test results have shown that state-of-the-art high-concentration concentrator photovoltaic (CPV) modules and systems using MJ cells produce module conversion efficiencies greater than 30%, based on direct normal irradiance (DNI) to the module aperture [6–9]. CPV technology is advantageous for high-DNI regions but is not currently attractive for midrange-DNI regions, where the ratio of direct (beam) sunlight to global sunlight is not very high, because high-concentration optics cannot concentrate diffuse sunlight to solar cells because the acceptance angle is limited [10]. If high-concentration CPV modules can harvest diffuse sunlight too, they can potentially produce the

highest module conversion efficiency, i.e. the highest energy yield per unit area, even in midrange-DNI regions. Demonstrating this technological potential is an important step in the progress being made in photovoltaic engineering.

Hybrid CPV architectures in which an additional low-cost solar cell captures diffuse sunlight in a high-concentration CPV module have recently been proposed and studied. Benitez et al. [11] described a hybrid CPV module design for production of a high annual electrical energy density ( $\text{kWh}/(\text{m}^2 \text{ year})$ ) in a patent document. Their design involves a primary solar cell upon which direct normal radiation is concentrated by a concentrator and one or more auxiliary solar cells surrounding the primary cell that receive solar radiation from the concentrator that misses the primary cell. They have presented a schematic illustration of an example hybrid module design that uses a Fresnel lens as a typical concentrator.

Other types of hybrid module designs that do not use conventional Fresnel lenses (with the lens aperture, i.e. the aperture size of a single lens that varies from several centimeters to several tens of centimeters) but rather

miniaturized lenses and micro-scale solar cells selected to improve optical and thermal performance and reduce material consumption have been studied [12,13]. The results of ray-tracing analyses show that for a constant geometric concentration ratio to the primary cell, the optical efficiency of the hybrid module increases as the module's lens and cell become smaller, mainly because light absorption loss in the lens material decreases as the thickness and volume of the lens decrease. As an advanced miniature hybrid architecture, a micro-scale III–V cell (cell size: 250  $\mu\text{m}$ ) on a wide-area silicon substrate has been designed, and the results of a preliminary cost analysis, taking into consideration the fabrication process, have been reported [14].

In addition to the results of simulation-based studies, the results of experimental studies have been reported. Shultz et al. [15] carried out an outdoor experiment using a CPV module with a 3  $\times$  3 conventional Fresnel lens (lens aperture: 220  $\times$  220  $\text{mm}^2$ ) and a triple-junction (3J) cell (cell size: 10  $\times$  10  $\text{mm}^2$ ) as the primary cell. They characterized the irradiance distribution and spectral profile of diffuse sunlight inside the module using a charge coupled device (CCD) spectrometer via fiber-optic cable and suggested the use of a copper indium selenide (CIS) cell as the auxiliary cell. Yamada and Okamoto [16] fabricated a prototype hybrid module with a conventional Fresnel lens (lens aperture: 120  $\times$  120  $\text{mm}^2$ ), a 3J cell as the primary cell (cell size: 5.5  $\times$  5.5  $\text{mm}^2$ ), and a crystalline silicon (c-Si) cell as the auxiliary cell (cell size: 120  $\times$  120  $\text{mm}^2$ ), and demonstrated electricity generation using both solar cells. However, the auxiliary c-Si cell was not well integrated into the module in a practical manner; for example, the auxiliary c-Si cell was machined to make a hole through which concentrated sunlight would pass and hit the primary 3J cell. Yamada et al. also attempted to demonstrate the use of a miniature hybrid module with a non-Fresnel-type silicone lens (lens aperture: 15.4  $\times$  15.4  $\text{mm}^2$ ) and a primary 3J cell (cell size: 2.5  $\times$  2.5  $\text{mm}^2$ ) that is mechanically stacked on the bus bar at the surface of an auxiliary c-Si cell (9.8  $\times$  9.8  $\text{mm}^2$ ) [17]. A tentative outdoor experiment showed that higher energy yield could be attributed to the miniature architecture and the gain of c-Si cell. However, the module generated less electricity from diffuse radiation than expected because the c-Si cell size was smaller than the lens aperture size.

This paper builds upon the descriptions and analyses of similar systems in the literature [16,17] and provides performance data on module conversion efficiency with respect to various sunlight conditions from longer outdoor experiments, as a proof-of-concept demonstration of a hybrid CPV architecture. The miniature hybrid module design was updated to be smaller and more practical than in previous studies by using a non-Fresnel-type polymethyl methacrylate (PMMA) lens (lens aperture: 14.1  $\times$  14.1  $\text{mm}^2$ ) and smaller 3J cells (cell size: 1  $\times$  1  $\text{mm}^2$ ) for the primary cell. A wide-area bifacial c-Si cell was employed as an auxiliary cell to fully capture diffuse sunlight, not only from the module aperture side but also from the back side of the module, thereby maximizing the global normal irradiance (GNI)-based module conversion efficiency.

## 2. HYBRID CPV ARCHITECTURE

Figure 1 shows a conceptual schematic diagram of the hybrid CPV architecture. A high-efficiency concentrator solar cell (primary solar cell), such as a III–V MJ solar cell, and low-cost solar cells (auxiliary solar cells), such as c-Si solar cells, are combined into one photovoltaic module with concentrator optics. The low-cost cells are placed around the high-efficiency cell. In this arrangement, referred to as a “cell-in-cell arrangement,” beam sunlight is concentrated to the high-efficiency cell in the same manner as in a conventional CPV architecture. Simultaneously, diffuse sunlight—which is inevitably present at the Earth's surface, even in high-DNI regions, but cannot be concentrated to high-efficiency cells at high concentration ratios because of the limits of solar concentration—is captured and harvested by the low-cost solar cells. If the low-cost cells are of the bifacial type, the diffuse sunlight reflected from the ground surface and/or building surfaces can also be captured by the back sides of the bifacial cells. It should be noted that in this concept there are two independent currents from the beam and the diffuse irradiation because current matching between the primary cells and the auxiliary cells is difficult under actual conditions of fluctuating sunlight.

According to the literature [1], a high solar concentration on an MJ solar cell with a large number of junctions leads to high conversion efficiency. Thus, converting concentrated beam sunlight into electricity using a high-efficiency but expensive solar cell with minimal cell area and simultaneously converting diffuse sunlight into electricity using an inexpensive solar cell with a large cell area is a method of maximizing the energy yield of terrestrial photovoltaic conversion.

## 3. FABRICATION AND EXPERIMENT

Figure 2 illustrates the design of a prototype hybrid CPV mini-module incorporating a GaInP/GaInAs/Ge 3J cell

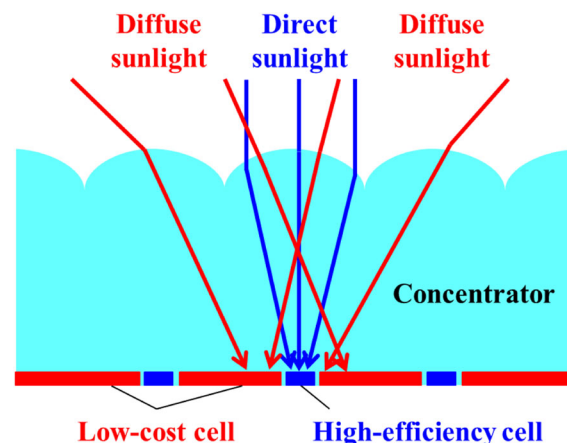
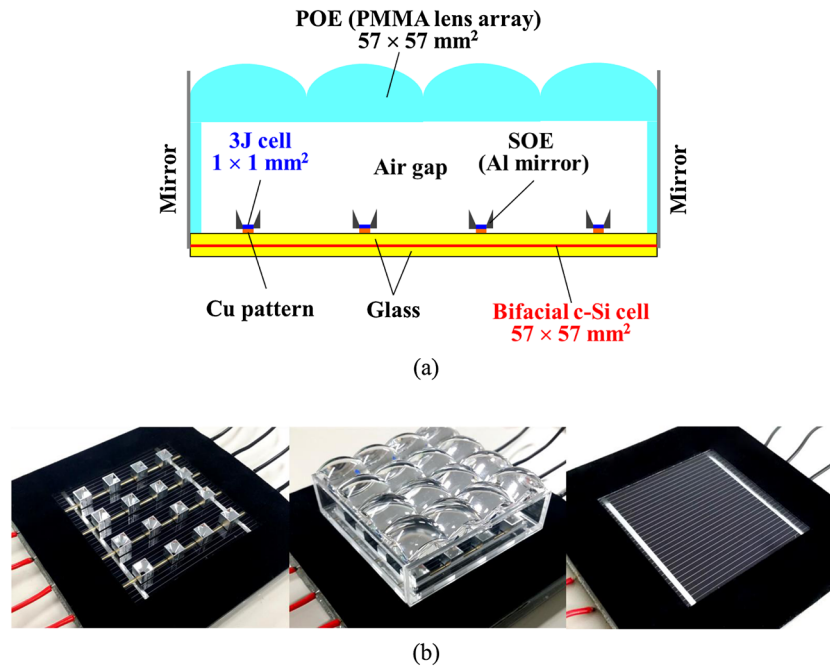


Figure 1. Conceptual schematic diagram of hybrid CPV architecture.



**Figure 2.** Hybrid CPV mini-module design. (a) Schematic diagram of cross section of the mini-module. (b) Photographs of the mini-module (left: without POE, center: with POE, right: back side view).

and a bifacial mono c-Si cell, both of which are commercially available. The 3J cell was packed in a package that was originally used for light-emitting diode (LED) chip packaging. As a result, the package had both anode and cathode terminals on its back side, which made it possible for a robotic machine to mount the package quickly and accurately and to solder the package onto a metal (Cu) wiring pattern fabricated on a transparent glass substrate. This type of automated mounting method is commonly used in mass production processes for various electronic devices and is called surface-mount technology (SMT). The area of the wiring pattern was minimized to ensure high transmittance of the diffuse sunlight to the c-Si cell. The module of the aperture area was  $57 \times 57 \text{ mm}^2$ , and the geometric concentration ratio was approximately 200X for the 3J cell, which had an active area of approximately  $1 \text{ mm}^2$  (this was the smallest 3J cell that the authors could purchase).

Assuming similarity of shape and configuration for the lens and cell, i.e. for the same geometric concentration ratio with the same lens and cell geometry, using a smaller cell decreases the concentrator volume, i.e. the focal length and lateral size of the lens. Hence, light attenuation (absorption loss) when the light travels in the lens medium can be reduced. The cell temperature can also be reduced for the same geometric concentration ratio, mainly because of rapid lateral heat dissipation from small cells [12,18]. In addition, the amount of lens material used in the miniature hybrid module can be reduced.

The major drawbacks of a miniature design are the following. (i) A large number of cells must be accurately mounted in an array. A suitable production method must be developed to accomplish this. The SMT approach used

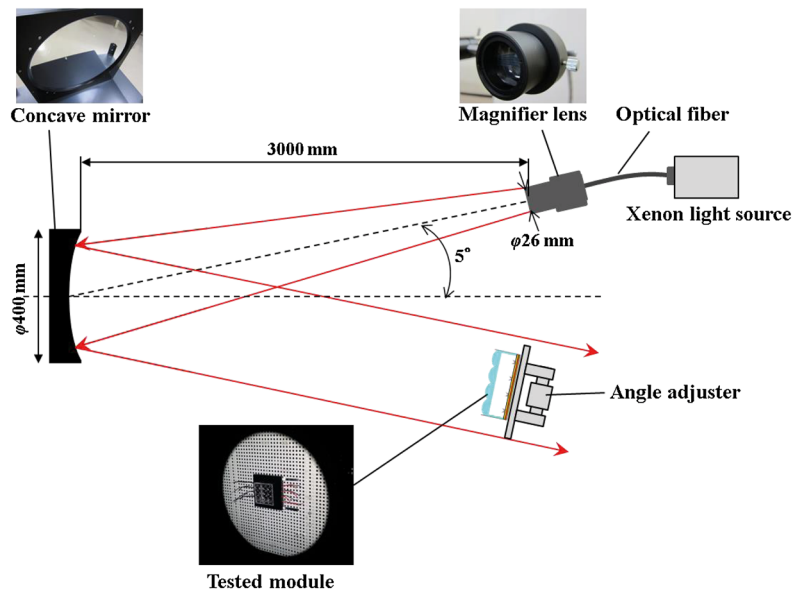
in this study is one possible solution to this problem. (ii) High accuracy is required for the concentrator shape and alignment [19]. This is especially true for higher concentration ratios, especially with a miniature Fresnel lens, in which prism edge must be sufficiently sharp to maintain concentration performance for a very small cell.

In this study, to avoid the difficulty of fabricating an accurate miniature Fresnel lens, a non-Fresnel type  $4 \times 4$  lens array made of a PMMA resin was used as the primary optical element (POE), with a reflective secondary optical element (SOE) used to give the module a large acceptance angle [20]. Although a lens without an air gap between the lens and the cell would have had less optical loss, we purposely separated the lens from the glass substrate with an air gap to facilitate access to and maintenance of the SOE and 3J cells. The bifacial c-Si cell, which was cut from a 6-inch commercial cell, was laminated on the back side of the glass substrate to capture diffuse sunlight on the back side as well as through the lens aperture. Transparent silicone was used for the lamination. The silicone layer was approximately 0.1 mm thick (not shown in Figure 2). The cell size of the bifacial c-Si cell was the same as that of the POE lens ( $57 \times 57 \text{ mm}^2$ ) on both the front and back sides; however, 25.5% of the front-side area of the bifacial cell was shaded by the SOEs, 3J cells, and wiring pattern. To establish a periodic boundary condition, the four side-walls of the module were surrounded by high-reflection flat mirrors with a specular reflectance of 0.85 over the solar spectrum. These mirrors approximately emulate the optical conditions of infinitely large lens-cell arrays, i.e. they emulate incoming and outgoing rays to and from the neighboring lens-cell array as a result of multiple reflections

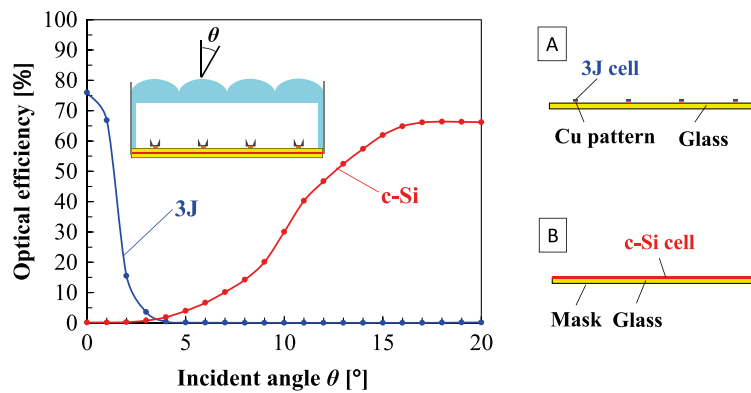
and refractions of incident sunlight. It should be noted that the series-connected 3 J cell and c-Si cell were electrically separated; both cells had independent output terminals.

Figure 3 shows the experimental setup and the result of the incident angle dependency of the prototype mini-module. Investigating the incident angle dependency of the optical efficiency of a hybrid module is an important step in the further improvement of the optical design. In this study, the optical efficiency of the module for each solar cell was defined as the angular optical transmission of the module components for each solar cell built into the mini-module—in other words, the ratio of the light energy

that reaches each solar cell to the light energy incident on the module aperture. The incident light energy is attenuated by reflection losses at lens–air interfaces and the SOE mirror, absorption loss inside the lens material, misalignment of the optical element, and design error in the optical element shape. The optical efficiency was measured under highly collimated artificial sunlight created by a solar simulator constructed by the researchers, as shown in Figure 3 (a). The simulator consists of a xenon light source, a 400-mm-diameter concave mirror, and a magnifier lens that is connected to the xenon light source via optical fiber [21]. The collimation angle of the artificial



(a)



(b)

**Figure 3.** Indoor measurement for the incident angle dependency of the optical efficiency of the module for 3 J cell and c-Si cell. (a) Experimental setup of highly collimated artificial sunlight. (b) Measurement results labeled “3 J” and “c-Si” represent the optical efficiencies of the module for the 3 J cell and c-Si, respectively. Supplemental figures A and B show the configuration of the reference cell for the 3 J cell and c-Si, respectively. It is noted that 0.1-mm-thick transparent silicone layer is present at the upper surface of the c-Si cell.

sunlight was measured by a method described in the literature [22]. The simulator had a collimation angle within  $\pm 0.2^\circ$ , which is smaller than the view angle of the sun ( $\pm 0.27^\circ$ ). The uniformity at an irradiated area 150-mm square and the temporal stability satisfied the Class A specification of the IEC 60904-9 Edition 2 standard. The irradiance was as low as 0.01 sun ( $10 \text{ W/m}^2$ ). The spectral composition of the artificial light was evaluated by spectral matching ratio (SMR), which is defined as the ratio between the top and middle subcell photogenerated currents under the artificial sunlight, divided by that ratio under the AM1.5D standard spectrum [23–25]. SMR was measured by using a set of component reference cells (also known as “isotype” cells) in the same manner as described in the literature [25]. The measured SMR was 0.88, meaning that the current-limiting cell was expected to be the top cell in cases without concentrating optical elements.

The optical efficiency for the 3J cell at certain incident angle was estimated as the ratio of the measured short-circuit current of the 3J cell when it was built into the mini-module, as shown in Figure 2, to that of the same 3J cell when the lens and SOE were removed, as shown in supplemental figure A in Figure 3 (b). The optical efficiency for the c-Si cell was estimated as the ratio of the measured short-circuit current of the c-Si cell when it was built into the mini-module, as shown in Figure 2, to that of the same c-Si cell when the lens, SOE, and glass substrate were removed, as shown in supplemental figure B in Figure 3 (b). It should be noted that a 0.1-mm-thick transparent silicone layer, which had a refractive index similar to that of the glass substrate, was still present at the upper surface of the c-Si cell.

Because of the thick POE lens used and alignment errors associated with the lens and cells, the peak optical efficiency for the 3J cell was as low as 76% at normal incidence and dropped at  $\theta \sim 2^\circ$ . In contrast, the optical efficiency for the c-Si cell was nearly zero at normal incidence and increased steeply as the incident angle increased, up to 66% at  $\theta \sim 20^\circ$ . It was confirmed that the optical efficiency for the c-Si cell was nearly constant for  $20^\circ \leq \theta < 90^\circ$ , although this is not shown in Figure 3 (b).

Assuming that actual diffuse sunlight has an isotropic angular distribution, hemispherical integration of the measured angular optical efficiency for isotropic diffuse sunlight is estimated to be  $\sim 65\%$ . Incident light in the range of  $2.5^\circ < \theta < 16^\circ$  escaped without being captured by either cell. This is because a large portion of the incident light is reflected by the SOE, which exits the module. This implies that the optical efficiency of the prototype mini-module can be further improved if the amount of light that escapes can be reduced by a better optical design, although the performance of the module was sufficient for the success of the proof-of-concept demonstration.

Figure 4 shows photographs of the prototype mini-module mounted on a two-axis sun tracker and the measurement instruments. We carried out the outdoor experiments with and without a masking shield on the back side of the bifacial c-Si cell surface to assess the contribution of the back side gain to the electricity generation of the bifacial cell. For the experiment conducted with the masking shield in place (i.e. the single-sided case), the mini-module was configured as shown in Figure 4 (a). For the experiment without the masking shield in place (i.e. the bifacial case), the mini-module was configured as shown in Figure 4 (b). A gray-colored paper with hemispherical diffuse reflectance on the AM1.5G standard spectrum of  $\sim 0.37$  was placed on the opposite surface of the bifacial c-Si cell (the view factor from the c-Si cell aperture to the gray-colored paper was 0.35) to ensure moderate reflection and prevent unexpected excess irradiation input to the back side of the c-Si cell during the experiment.

It should be noted that the reflectance of ground surfaces varies widely, from approximately 0.1 for dark wet soil to approximately 0.9 for fresh snow, depending on the materials and surface conditions. The typical reflectance of soil, glass, and sand is less than approximately 0.4. Concrete has a slightly higher reflectance of approximately 0.5 [26]. In the actual operation of a CPV tracker array, the module inclination angle and the reflectance of surrounding objects, such as neighboring trackers and buildings, will also affect the gain at the back side of the bifacial cell.

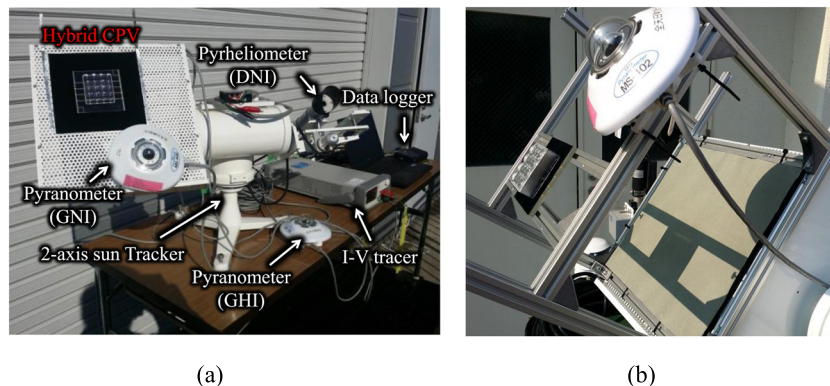


**Figure 4.** Photographs of setup for outdoor experiment. (a) Overview for single-sided experiment, (b) module setup for bifacial experiment.

The current–voltage ( $I$ – $V$ ) curves of the series-connected 3 J cells and c-Si cell were determined independently using current and voltage measurements obtained using a two-channel  $I$ – $V$  tracer. The back side of the bifacial cell was shaded when the contribution of the back-side electricity generation was evaluated separately. The GNI and DNI were measured using a pyranometer and a pyrliometer, respectively, both of which were mounted on the sun tracker. The global horizontal irradiance (GHI) was also measured using another pyranometer. The specifications of the measurement system are summarized in Table I.

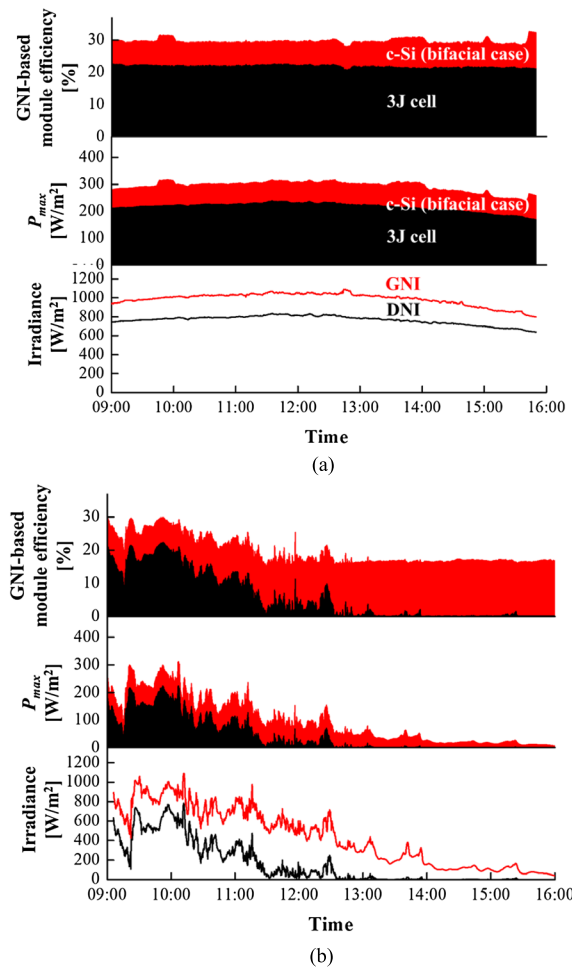
Figure 5 shows the measured daily variation of the maximum power  $P_{\max}$  of both cells and the GNI-based module conversion efficiency for the corresponding solar irradiance data.  $P_{\max}$  was normalized to watts per unit module aperture area. As Figure 5 (a), shows, in clear-sky conditions, the 3 J cell generated the most power (73.7% of the daily total power generation). In contrast, as Figure 5 (b) shows, in partially cloudy conditions, the 3 J cell lost power when the DNI decreased, and the bifacial c-Si cell generated power from diffuse sunlight. It should be noted that even in clear-sky conditions, the bifacial c-Si cell constantly generated electricity and thus contributed to improvement of the module efficiency.

Figure 6 (a) shows the relationship between the GNI-based module conversion efficiency and the diffuse-to-global ratio obtained from the measured daily variations, based on 12 days of measurements obtained during April and May 2015 at the Nagaoka University of Technology in Japan. The diffuse-to-global ratio  $\gamma$  is defined as  $\gamma = (\text{GNI} - \text{DNI}) / \text{GNI}$ . A larger  $\gamma$  indicates a larger diffuse component fraction, and  $\gamma = 1.0$  indicates that the module aperture receives only diffuse sunlight. For  $\gamma = 0.19$ , the hybrid CPV module, in which the  $P_{\max}$  of the c-Si cell was added to that of the 3 J cells, achieved a GNI-based module efficiency of  $\eta = 32.7\%$  in the bifacial case and  $\eta = 29.4\%$  in the single-sided case. On the other hand, that of the conventional CPV module, in which only the  $P_{\max}$  of the 3 J cells was counted, was limited to  $\eta = 23.7\%$ , although the DNI-based module efficiency was 29.3%.

Figure 6 (a) also shows that the GNI-based module efficiency depends on the value of  $\gamma$  and that the efficiency of the hybrid CPV module is greater than that of a conventional CPV module for any  $\gamma$  values and greater than the module efficiency range of current commercial flat c-Si

**Table I.** Specifications of measurement instruments.

Measurement instruments		Specification
Pyranometer	EKO MS-402	ISO9060
		First class
Pyrliometer	EKO MS-54	ISO9060 First class, View angle 5°
Sun tracker	EKO STR-22	Tracking accuracy <0.01°
I–V tracer	Agilent B2902A	Dual channel



**Figure 5.** Daily variation of GNI-based module conversion efficiency of the hybrid CPV mini-module,  $P_{\max}$ , GNI, and DNI. (a) Clear-sky day (30 April 2015). (b) Partially cloudy day (18 May 2015).

modules (approximately 17%) for  $\gamma \leq 0.73$ . In contrast, the conventional CPV module achieved better module efficiency than the current flat c-Si module at  $\gamma \leq 0.39$ .

The bar graph in Figure 6 (b) shows the average power generation per module aperture area in eight  $\gamma$ -bins for the 3 J-only case, the single-sided case, and the bifacial case. The plots show the values of the improvement factor, defined as  $(P_{3J} + P_{c-Si}) / P_{3J}$ , for the single-sided case and the bifacial case. Here,  $P_{3J}$  and  $P_{c-Si}$  represent the average power generation by the 3 J cell and the c-Si cell in each bin, respectively. The improvement factor tends to increase as  $\gamma$  increases, i.e. as the diffuse component fraction increases, in both cases. This trend is emphasized in the bifacial case. On the other hand, the gain in the average power generation tends to be larger as  $\gamma$  decreases because the amount of sunlight increases as the DNI increases. The bifacial cell increases the power by factor of 1.39 at high-DNI conditions ( $\gamma \leq 0.25$ ) and by factor of 1.63 at midrange-DNI conditions ( $0.4 \leq \gamma \leq 0.5$ ). These results

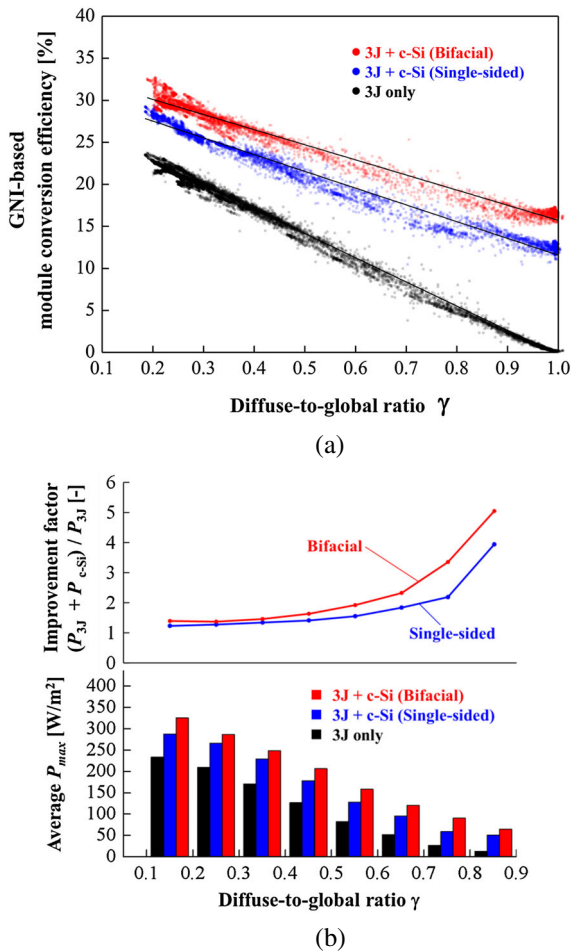


**Figure 6.** Results based on 12-day outdoor experiment during April–May 2015 in Japan. (a) GNI-based module conversion efficiency. (b) Average generated power and improvement factor (bifacial case and single-sided case).

suggest that the addition of a low-cost solar cell to the high-concentration CPV architecture to capture diffuse sunlight can increase the energy yield in both the high- and midrange-DNI regions.

The highest DNI-based module efficiency of a conventional non-hybrid CPV module reported in the literature [6] is 36.7%, obtained by a module with a Fresnel lens and a four-junction cell at concentrator standard test conditions [IEC62670-1]. If we assume the same DNI-based module efficiency for beam sunlight conversion of a hybrid CPV module and also assume the same relative efficiency improvement at  $\gamma=0.19$  from a non-hybrid architecture to the hybrid architecture obtained experimentally as shown in Figure 6, we can expect a GNI-based module efficiency of  $\eta=41.0\%$  in the bifacial case and  $\eta=36.8\%$  in the single-sided case. In contrast, the GNI-based module efficiency of the non-hybrid CPV module is limited to 29.7%.

Meanwhile, a flat non-concentration module composed of MJ cells, which are typically designed and used in space applications, also has the potential to achieve high GNI-

module efficiency over a broad  $\gamma$  range in terrestrial applications. The highest reported efficiency of MJ cells for 1 sun application is 38.8% [3]. The highest reported c-Si cell efficiency is 25.6%, and the highest reported c-Si module efficiency is 22.9% [3]. Thus, the ratio of the c-Si module efficiency to the cell efficiency ratio is  $\sim 0.88$ . Assuming the same ratio for a 38.8%-efficient MJ cell, a GNI-based module efficiency of  $\sim 34\%$  could be feasible. The nominal cell efficiency of currently available MJ solar cells for 1 sun space application is 27–30%, based on information provided by manufacturers [27–30]. However, in such a flat MJ module, the cell area must be nearly the same as the module aperture area, which causes a drastic increase in the module cost.

As mentioned above, the hybrid CPV architecture has an advantage over the conventional non-hybrid CPV architecture and the flat MJ module in terms of its GNI-based module efficiency. The major drawbacks of the present hybrid concept are as follows. (i) Two independent currents are generated from direct and diffuse sunlight. A suitable inverter system is necessary to treat those two independent currents with independent maximum power point tracking. (ii) There is a higher cost associated with the use of an extra cell for diffuse irradiation. The bifacial extra cell contributes to improving the module efficiency in comparison to a single-sided extra cell; however, it also increases the cost. The type and structure of the extra solar cell should be optimized for the conversion of the diffuse radiation of irradiation less than 1 sun because the extra cell only captures diffuse sunlight and should be lower in cost than the conventional solar cell for a 1-sun application.

## 4. CONCLUSIONS

In this study, the potential of integrating a low-cost bifacial solar cell into a high-concentration CPV architecture to harvest diffuse sunlight was demonstrated experimentally. For high-DNI conditions, the bifacial crystalline silicon solar cell placed below the triple-junction solar cell in the prototype mini-module enhanced the generated power by a factor of 1.39, and the resultant GNI-based module efficiency achieved was 32.7%. For midrange-DNI conditions, the generated power was increased by a factor of 1.63, and the resultant GNI-based module efficiency achieved was 25.6%. The results of this study show that the proposed hybrid CPV architecture has the potential to maximize energy yield by photovoltaic conversion in terrestrial applications in which diffuse sunlight, including the reflection of sunlight from the ground surface and surrounding objects, is inevitable. Given that the results of the present study were obtained at a single location in Japan, in a midrange-DNI region, the trends in the power enhancement and module efficiency should be expected to be different at different locations, depending on the solar radiation conditions. Further research and development

are required to optimize the module structure and minimize its cost.

## ACKNOWLEDGMENT

This work was supported by JSPS KAKENHI Grant Number 26289373.

## REFERENCES

- Kurtz S, Myers D, McMahon WE, Geisz J, Steiner M. A comparison of theoretical efficiencies of multi-junction concentrator solar cells. *Progress in Photovoltaics: Research and Applications* 2008; **16**: 537–546. DOI:10.1002/pip.830.
- Research cell efficiency records. Natl Renew Energy Lab. <http://www.nrel.gov/ncpv/> (accessed December 22, 2015).
- Green MA, Emery K, Hishikawa Y, Warta W, Dunlop ED. Solar cell efficiency tables (version 47). *Progress in Photovoltaics: Research and Applications* 2016; **24**: 3–11. DOI:10.1002/pip.2728.
- King R, Bhusari D, Larrabee D. Solar cell generations over 40% efficiency. *Progress in Photovoltaics: Research and Applications* 2012; **20**: 801–815. DOI:10.1002/pip.1255.
- Ermer JH, Jones RK, Hebert P, Pien P, King RR, Bhusari D, Brandt R, Al-Taher O, Fetzer C, Kinsey GS, Karam N. Status of C3MJ+ and C4MJ production concentrator solar cells at spectrolab. *IEEE Journal of Photovoltaics* 2012; **2**: 209–213. DOI:10.1109/JPHOTOV.2011.2180893.
- Steiner M, Bösch A, Dilger A, Dimroth F, Dörsam T, Müller M, Hornung T, Siefert G, Wiesenfarth M, Bett AW. FLATCON® CPV module with 36.7% efficiency equipped with four-junction solar cells. *Progress in Photovoltaics: Research and Applications* 2015; **23**: 1323–1329. DOI:10.1002/pip.2568.
- Ghosal K, Lilly D, Gabriel J, Whitehead M, Seel S, Fisher B, Wilson J, Burroughs S. Semiprism field results and progress in system development. *IEEE Journal of Photovoltaics* 2014; **4**: 703–708. DOI:10.1109/JPHOTOV.2013.2288026.
- Friedman DJ, King RR, Swanson RM, McJannet J, Gwinner D. Editorial: Toward 100 gigawatts of concentrator photovoltaics by 2030. *IEEE Journal of Photovoltaics* 2013; **3**: 1460–1463. DOI:10.1109/JPHOTOV.2013.2270341.
- Kinsey GS, Bagiński W, Nayak A, Liu M, Gordon R, Garboushian V. Advancing efficiency and scale in CPV arrays. *IEEE Journal of Photovoltaics* 2013; **3**: 873–878. DOI:10.1109/JPHOTOV.2012.2227992.
- Winston R, Miñano JC, Benítez P, Shatz N, Bortz JC. *Nonimaging Optics*. Academic Press, 2005.
- Benitez P, Miñano J, Alvarez R. Photovoltaic concentrator with auxiliary cells collecting diffuse radiation. US Pat App 12/622,664 2009;1.
- Yamada N, Ijro T, Goto W, Okamoto K, Dobashi K, Shiobara T. Development of silicone-encapsulated CPV module based on LED package technology. 2013 IEEE 39th Photovolt. Spec. Conf., 2013, p. 0493–0496. doi:10.1109/PVSC.2013.6744197.
- Haney MW, Gu T, Agrawal G. Hybrid micro-scale CPV/PV architecture. Photovolt. Spec. Conf. (PVSC), 2014 IEEE 40th, 2014, p. 2122–2126. doi:10.1109/PVSC.2014.6925343.
- Paap S, Gupta V, Tauke-Pedretti A, Resnick P, Sanchez C, Nielson G, Cruz-Campa J.L., Jared B, Nelson J, Okandan M, Sweatt W. Cost analysis of flat-plate concentrators employing microscale photovoltaic cells for high energy per unit area applications. Photovolt. Spec. Conf. (PVSC), 2014 IEEE 40th, 2014, p. 2926–2929, 8–13 June 2014. doi:10.1109/PVSC.2014.6925544.
- Schultz RD, van Dyk E., Vorster F. The potential of using diffuse light in concentrator photovoltaic modules for enhanced energy production. EU PVSEC 2013 Conf. proceedings, 2013, p. 1CV.6.30.
- Yamada N, Okamoto K. Experimental measurements of a prototype high concentration Fresnel lens CPV module for the harvesting of diffuse solar radiation. *Optics Express* 2014; **22**(Suppl 1): A28–34. DOI:10.1364/oe.22.000a28.
- Okamoto K, Hirai D, Yamada N. Design and test of cell-in-cell-structured CPV modules for better solar energy conversion. Tech. Dig. 6th World Conf. Photovolt. Energy Convers., 2015, 5TuPo.9.14.
- Arase H, Matsushita A, Itou A, Asano T, Hayashi N, Inoue D, Futakuchi R, Inoue K, Nakagawa T, Yamamoto M, Fujii E, Anda Y, Ishida H, Ueda T, Fidaner O, Wiemer M, Ueda D. A novel thin concentrator photovoltaic with microsolar cells directly attached to a lens array. *IEEE Journal of Photovoltaics* 2014; **4**: 709–712. DOI:10.1109/JPHOTOV.2013.2292364.
- Jared BH, Saavedra MP, Anderson BJ, Goeke RS, Sweatt WC, Nielson GN, Okandan M, Elisberg B, Snively D, Duncan J, Gu T, Agrawal G, Haney MW. Micro-concentrators for a microsystems-enabled photovoltaic system. *Optics Express* 2014; **22**: A521. DOI:10.1364/OE.22.00A521.
- Jaus J, Bett AAW, Reinecke H, Weber ER. Reflective secondary optical elements for fresnel lens based concentrator modules. *Progress in Photovoltaics: Research and Applications* 2011; **19**: 580–590. DOI:10.1002/pip.1065.

21. Yamada N, Kiryu M, Yoshida T, Ijiro T, Okamoto K. Test of prototype highly-collimated/low-irradiance solar simulator for brief optical evaluation of solar concentrator system (in Japanese). *Journal Japan Solar Energy Society* 2012; **38**: 39–46.
22. Yamada N, Okamoto K, Ijiro T, Kiryu M, Yoshida T. Flash xenon CPV simulator with low-cost elastic bent-trough mirrors. 9th Int. Conf. Conc. Photovolt. Syst. (CPV-9), Miyazaki (April 15–17, 2013), AIP Conf. Proc., vol. 168, 2013, p. 168–171. doi:10.1063/1.4822223.
23. Muller M, Kurtz S, Rodriguez J. Procedural considerations for CPV outdoor power ratings per IEC 62670. 9th Int Conf Conc Photovolt Syst (CPV-9), Miyazaki (April 15–17, 2013), AIP Conf Proc 2013;7:125–128. doi:10.1063/1.4822214.
24. Victoria M, Herrero R, Domínguez C, Antón I, Askins S, Sala G. Characterization of the spatial distribution of irradiance and spectrum in concentrating photovoltaic systems and their effect on multi-junction solar cells. *Progress in Photovoltaics: Research and Applications* 2013; **21**: 308–318. DOI:10.1002/pip.1183.
25. Domínguez C, Antón I, Sala G, Askins S. Current-matching estimation for multijunction cells within a CPV module by means of component cells. *Progress in Photovoltaics: Research and Applications* 2013; **21**: 1478–1488. DOI:10.1002/pip.2227.
26. McEvoy A, Markvart T, Castaner L. *Practical Handbook of Photovoltaics*, Second edn. Fundamentals and Applications. Academic Press, 2011.
27. Spectrolab, Inc. <http://www.spectrolab.com/solarcells.htm> (accessed December 25, 2015).
28. AZUR SPACE Solar Power GmbH. <http://www.azurspace.com/index.php/en/products/products-space/space-solar-cells> (accessed December 25, 2015).
29. SolAero Technology Corporation. <http://solaerotech.com/products/space-solar-cells-coverglass-interconnected-cells-cic/> (accessed December 25, 2015).
30. EMCORE corporation. <http://www.emcore.com/ztj-space-solar-cell/> (accessed December 25, 2015).